

Supplementary Information for

Resolving Local Configurational Contributions to X-ray and Neutron Scattering Radial Distribution Functions Within Solutions of Concentrated Electrolytes – A Case Study of Concentrated NaOH

David Semrouni,^{*1} Hsiu-Wen Wang,^{*2} Sue B. Clark,^{1,4} Carolyn Pearce,⁴ Katharine Page,³ David J. Wesolowski,² Andrew G. Stack,² Aurora E. Clark^{1,4}

¹Department of Chemistry and the Materials Science and Engineering Program, Washington State University, Pullman, WA 99164

²Chemical Sciences Division, Oak Ridge National Laboratory, Oak Ridge, TN 37831

³Neutron Scattering Division, Oak Ridge National Laboratory, Oak Ridge, TN 37831

⁴Pacific Northwest National Laboratory, Richland, WA 99352

*indicates first authors

corresponding authors: david.semrouni@wsu.edu, wangh3@ornl.gov, auclark@wsu.edu

Section I) Detailed Information:

I.1 Description of Diffraction Data Reduction Methods. For neutron scattering measurements, detectors were calibrated with scattering from a diamond powder sample, data were normalized against scattering from a vanadium rod, and the container background was subtracted. The resultant total scattering structure factor, $S(Q)$ can be written as:

$$S(Q) = \sum_{i=j} (c_i b_i)^2 [S_{ii}(Q) - 1] + \sum_{i \neq j} 2(c_i c_j b_i b_j) [S_{ij}(Q) - 1]$$

where c_i is atomic fraction and b_i is coherent scattering length of atom i . In the case of X-ray scattering, b_i is the Q-dependent atomic form factor $f_i(Q)$. Data were transformed to a PDF $g(r)$, using the specific IDL codes developed for the NOMAD instrument.¹ The relationship between $S(Q)$ and $g(r)$ is:

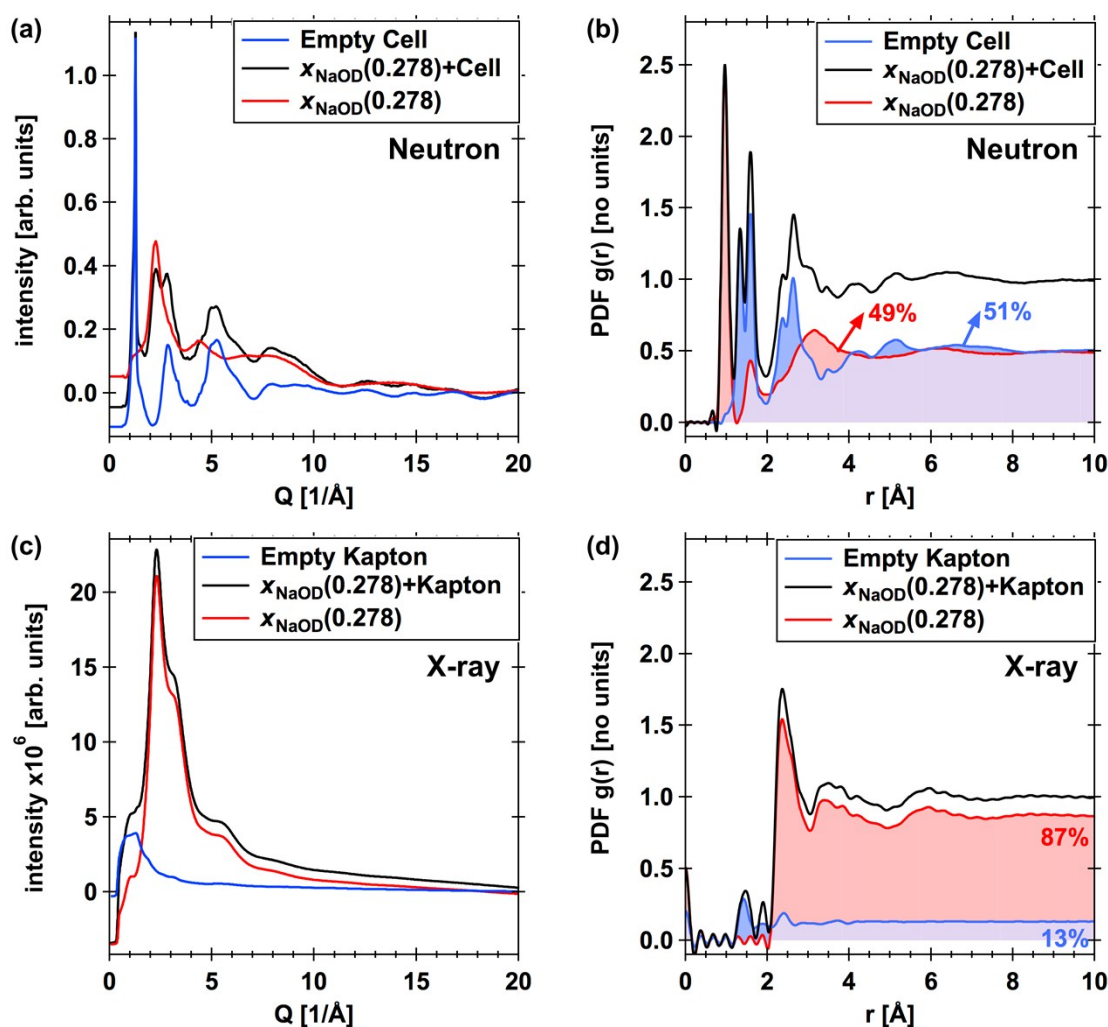
$$g(r) = 1 + [1/(2\pi^2 r \rho_0)] \int_0^{Q_{max}} Q [S(Q) - 1] \sin(Qr) dQ$$

For the X-ray scattering measurements, the program Fit2D² was used to calibrate the sample to detector distance and detector alignment with data from a CeO₂ powder standard. Raw scattering data was integrated into Q -space, applying a mask and polarization correction during integration. The normalized $S(Q)$ were produced in PDFgetX2³ by subtracting the polyimide container scattering, utilizing the appropriate sample composition, and applying standard corrections for the area detector setup.⁴

In both cases, the data was normalized with respect to the known composition and density (Table 1, S2). Neutron PDF $g(r)$ were calculated via Fourier transformation of the total scattering

data utilizing a Q maximum of 40 \AA^{-1} and a Lorch modification function⁵ was applied. Incoherent scattering from D was removed by subtracting real space intensity less than 0.7 \AA through Fourier filter methods.^{6,7} Measurements corresponding to a $x_{\text{NaOD}} = 0.278$ sample are shown in Figure S1 with measured scattering data in black, background scattering data in blue, and solution data (with background substraction) in red. The empty sample cell (PTFE+NMR) (blue) and $x_{\text{NaOD}} (0.278)$ solution (red) signals correspond to 0.51 and 0.49, of the measured total scattering intensity (in black), respectively. While this level of background scattering is significant, the final sample scattering signal is recovered well with the data reduction procedures.

Figure S1. (a) Neutron and (c) X-ray total scattering intensities for empty sample cell measurements (blue), NaOD ($x_{\text{NaOD}} = 0.278$) plus sample cell measurements (black), and resulting corrected (background subtracted) NaOD sample (red). Corresponding neutron (b) and X-ray (d) pair distribution functions $g(r)$ for the same series.



For the X-ray data, a Q maximum of 20 \AA^{-1} is used to produce $g_{\text{tot}}(r)$, and Compton scattering is corrected by subtracting real-space intensities less than 1.3 \AA through similar Fourier filter methods.⁶ Figure S1 displays the raw X-ray scattering intensities with the polyimide sample

tubing in blue, and the sample within the polyimide tubing in black. The background subtracted sample scattering is shown in red. The intensities decrease dramatically at high- Q because the corrections of X-ray atomic scattering factor are not applied. Figure S1 shows the corresponding X-ray PDF $g(r)$ data for the series. The fraction of empty polyimide cell to NaOD solution in the measured signal corresponds to 0.13 and 0.87, respectively.

I.2 Additional Details on the Simulation Protocol. The SHAKE⁸ algorithm was used to maintain rigidity in H₂O and OH⁻ for the non-polarizable set of simulations (Table S1), while rigid body integration was used with the polarizable force field (Table S1). Alternating NPT and NVT thermodynamic ensembles were employed with a Nosé-Hoover thermostat and barostat for the NPT ensemble,^{9,10} respectively with coupling constants of 0.1 and 1.0 ps. A 1 fs time step was used via the velocity-Verlet integrator,¹¹ with Ewald summation having a relative accuracy of 10⁻⁶ and a truncation in the real space of 12 Å. Similarly, vdW interactions were computed with a cutoff distance of 12 Å. Both the pure water and mol fraction of NaOH of 0.245 were studied, with compositions indicated in Table S2.

Table S1. Intermolecular parameters^{27,29-32} for H₂O, Na⁺ and OH⁻. * q_{Hh} is not on H_h for this model.

	Polarizable	Nonpolarizable
Nonbonding terms		
ϵ_{Ow}	0.88257	0.0371
σ_{Ow}	3.18395	0.05975
ϵ_{Oh}		0.05975
σ_{Oh}		3.2
ϵ_{V1}	0.294135	
σ_{V1}	2.80	
ϵ_{V2}	0.294135	
σ_{V2}	2.40	
Charges		
q_{Ow}	1.7162 (-1.7162)	-0.8476
q_{Mw}	-1.1146	
q_{Hw}	0.5573	0.4238
q_{Oh}	0.202 (-1.432)	-1.3
q_{Hh}	0.230*	0.3
q_{Na}	1.6876 (-0.6876)	1.0

Table S2. Mole fraction, concentration (in molality *m*), average molar mass, density, and number densities in the NaOD/D₂O solution system measured in this work and employed within the classical molecular dynamics simulations.

Scattering Experiments	D₂O	NaOD
mole fraction $x_{\text{NaOD}}^{\text{a}}$	0.000	0.245
weight% (wt%)	0.000	40.00
concentration mole no		
Na ⁺	--	18.056
OD ⁻	--	18.056
D ₂ O	55.51	55.51
Total	55.51	91.621
molar mass (g/mole)	20.02	20.20
density (<i>d</i> ; g/cm ³) ^b	1.111	1.551
no. density (ρ_n ; #/Å ³) ^c	0.033	0.046
atom density (ρ_o ; #/Å ³) ^d	0.100	0.111
D ₂ O/Na ⁺ ratio	--	3.07
Molecular Dynamics Simulations		
$N_{\text{H}_2\text{O}}$	600	453
N_{NaOH}	0	147

a. Mole fraction is defined as $x_{\text{NaOD}} = N_{\text{NaOD}} / (N_{\text{NaOD}} + N_{\text{D}_2\text{O}})$, where N_i = number of species *i* in the system.

b. Density based on [Sipos et al. 2000 and Hellstrom and behler 2017] with a linear regression for the estimation of mass densities, considering atomic weights by different isotopes.

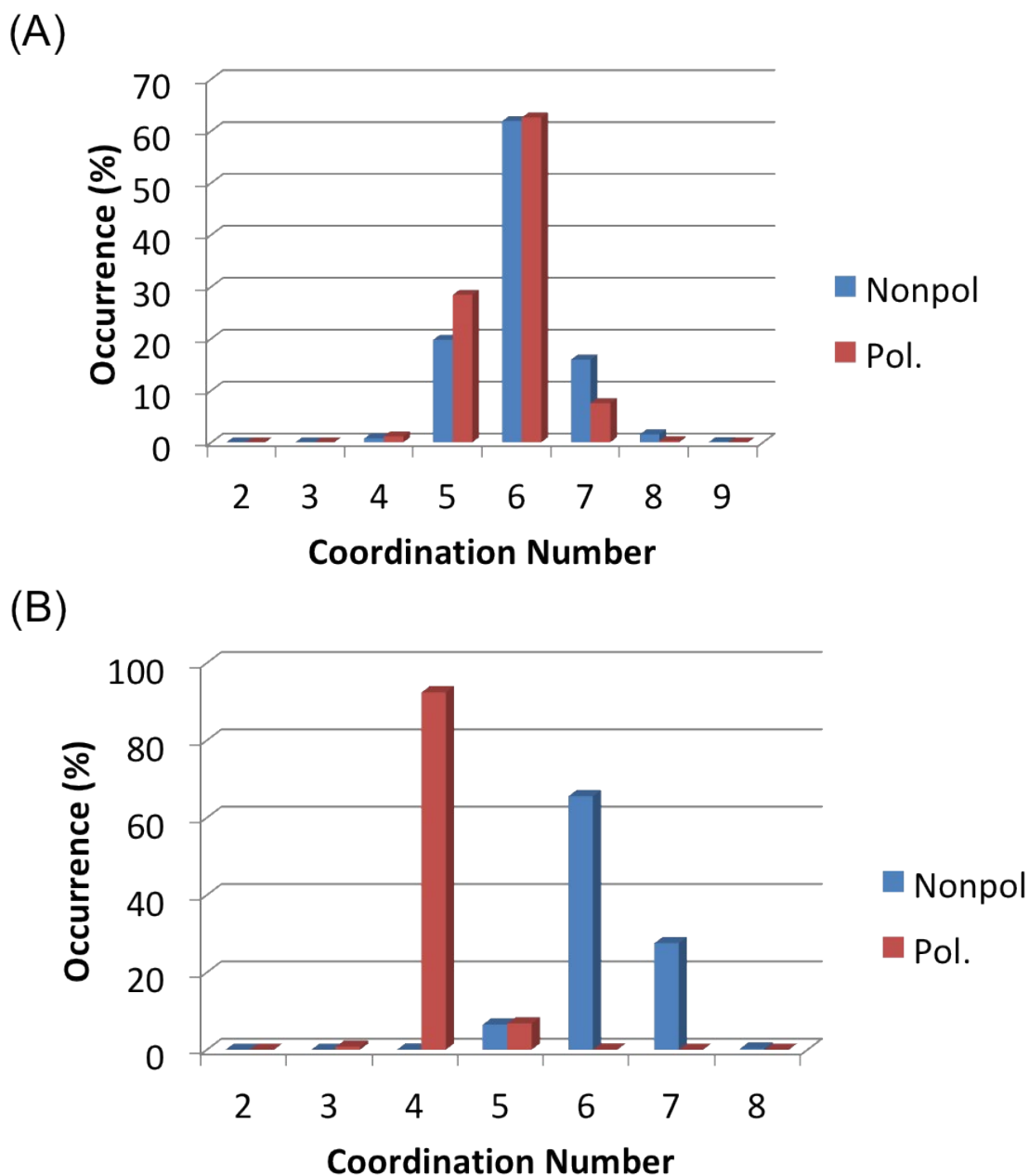
c. Number density is calculated according to $\rho_n = (N_A d / M) \times 10^{-24}$, where N_A is the Avogadro constant, *M* is solution's molar mass, and 10⁻²⁴ is the unit conversion factor from cm⁻³ to Å⁻³.

d. Atom density is calculated according to $\rho_o = \rho_n \times (1 - x_{\text{NaOD}} / (1 + x_{\text{NaOD}})) \times 3$

I.3 The Ability of Classical Potentials to Predict Na⁺ and OH⁻ Solvation Environments: In the infinite dilute limit, both polarizable and non-polarizable potentials predict similar solvation environments around Na⁺ (Figure S2), with water coordination number (CN) of 6 [i.e., Na(H₂O)₆⁺] approximately 60% of the time, followed by 20-28% for CN=5 and 6-8% for CN=7. This observation (using either force fields) is compatible with experimentally determined water CN of 4-6 from X-ray diffraction studies¹⁶⁻²¹ on various sodium-bearing aqueous solutions and agrees well with average water CN of 5.5 indicated by more recent studies of aqueous NaCl.²² In contrast, it is quite challenging for a classical force field to accurately depict hydroxide solvation. Studies have shown that, in a general, the hydroxide ion is a good HB acceptor. It accepts 3-4 HBs from water molecules (i.e., O_h···H_w) and weakly donates one to another water molecule near its hydrogen ion (i.e., H_h···O_w), forming a hypercoordinated solvation environment.^{21,23-25} The classical force fields tend to overestimate the water CN around O_h. For instance, as reported by [Marx 2010], the overcoordination of O_h with SPC/E water is observed in the infinitely dilute limit, with CN ranging from 6 (66%) to 7 (28%) around the hydroxide-O_h site. More sophisticated approaches, such as the charged ring model,²⁶ polarizability²⁷ and empirical valence bond²⁸ result

a better water CN (4-5) around the O_h site. In our polarizable model, at the infinitely dilute limit(?), a water CN of 4 around the O_h site is strongly favored proximately 90% of the time, such coordination is practically absent in the simple point-charge non-polarizable force field. We emphasize that many sophisticated potentials are generally parameterized for low concentrations (< 2 m) – an order of magnitude smaller than the solutions discussed in the present work.

Figure S2. Solvation environments about OH^- and Na^+ (a) and OH^- (b) in the infinite dilute limit predicted by polarizable and non-polarizable potentials



I.4 Simulation of the Neutron and X-ray Pair Distribution Functions. To obtain neutron radial distribution functions (nRDFs) and X-ray radial distribution functions (xRDFs), the MD derived distribution functions RDFs from simulation were weighted by ρ_0 defined in Tables 1 and S2, and as a function of the respective pair concentrations, and either the neutron scattering lengths b_i and b_j , or the X-ray atomic scattering factors b_i and b_j , of atoms i and j involved:

$$g_{N \text{ or } X}^{MD}(r) = \frac{1}{4\pi N \rho_0 r^2} \sum_i \sum_{j \neq i} \frac{b_i b_j}{\langle b \rangle^2} \delta(r - r_{ij})$$

where N is the number of atoms and ρ_0 is the atomic number density from the MD simulations. Neutron scattering lengths are taken from the literature,¹² while X-ray scattering factors are approximated using the equation¹³ the above Eqn. with coefficients c_i and a_{ik} taken for Na, O, and H from the literature as for fully charged species, Na^+ , O^{2-} , and H^+ (H/D is thus inactive).¹⁴ Here, we used b_D values to compute the nRDF. In the absence of proton transfer, the nature of isotope H/D does not significantly alter the RDFs.

$$b_i = c_i + \sum_{k=1}^4 a_{ik}$$

I.5 Additional Details on the first shell definition. The ChemNetworks¹⁵ software was used to, in terms of Graph Theory, determine networks of intermolecular interactions, where specific patterns are indicative of local composition and geometric environments. Each molecular entity, i.e. instance of water, hydroxide or sodium is considered as a node. Edges connect two nodes when distance and angle criteria shown in Table S3 are met. Each molecular entity possesses edges. Corresponding nodes define the first coordination shell of the central node (molecule). Averages and normalizations are operated to provide relative population of each first shell composition for sodium and deuterioxide.

Table S3. Geometric criteria defining an intermolecular edge in the layered interaction networks.

Node 1	Node 2	R_{cut} (Å)	Angle	Θ_{min} (°)	Θ_{max} (°)
O_w	H_w	2.50	$\angle \text{O}_w \text{H}_w - \text{O}_w$	0	180
H_w	O_w	2.50	$\angle \text{O}_w \text{H}_w - \text{O}_w$	0	180
O_w	H_h	3.10	$\angle \text{O}_h \text{H}_h - \text{O}_w$	0	180
O_h	H_w	2.30	$\angle \text{O}_h - \text{O}_w \text{H}_w$	0	180
O_w	Na^+	3.25	$\angle \text{H}_w \text{O}_w - \text{Na}$	0	180
O_h	Na^+	3.15	$\angle \text{H}_h \text{O}_h - \text{Na}$	0	180

I.6 Additional Details on cluster RDF. Once first shell compositions are sorted, we can isolate them and the corresponding interatomic pair distances are counted and summed for each instance of the same cluster composition. There is no absolute way to weight the RDF for non-

periodic system in the literature. In order to allow for a more consistent comparison between cluster RDFs of different composition, we attribute the corresponding bulk value to $\langle b \rangle^2$.

I.7 Additional Details on the molecular speciation in the HDNN snapshot. ChemNetworks was used to determine a covalent graph from atomic nodes. An O-H bond is considered present when the distance between an oxygen and a hydrogen is less than 1.3 Å. This threshold guarantees a number of hydroxide equal to the number of sodium cations in the system. Though it is convenient to be able to distinguish hydroxide from water, we would like to emphasize that this approach is limiting, considering that it does not capture the nature of transient species. A 1.3 Å long O-H bond is quite long for a canonical water molecule. Conversely, this distance is very short for an intermolecular hydrogen bond. Roughly, near 10% of excess hydrogen can be considered belonging to a transient species. This gives us an indication on the pertinence of hydroxide distinction from water and subsequent analyses we present in the current work.

Section II) Supporting Information for Results and Discussion:

Figure S3. (a) Experimental total scattering structure factor, $S(Q)$, for heavy water ($x_{\text{NaOD}} = 0$), (b) Corresponding pair distribution functions $g(r)$, (c) simulated neutron PDF of water with the polarizable and non-polarizable force fields, (d) simulated X-ray PDF of water with the polarizable and non-polarizable force fields.

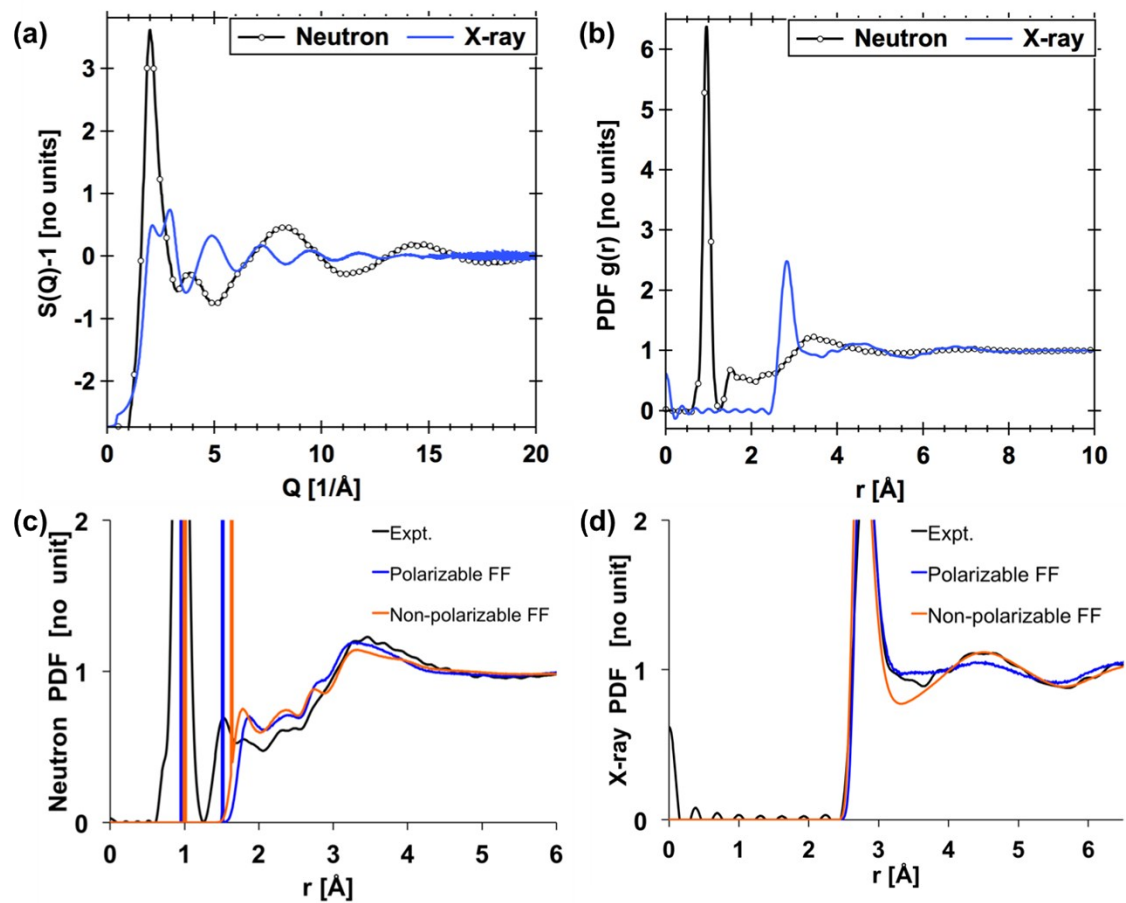


Figure S4. Experimental total scattering structure factor, $S(Q)$, for $\chi_{\text{NaOD}} = 0.245$ solutions as defined in Table 1.

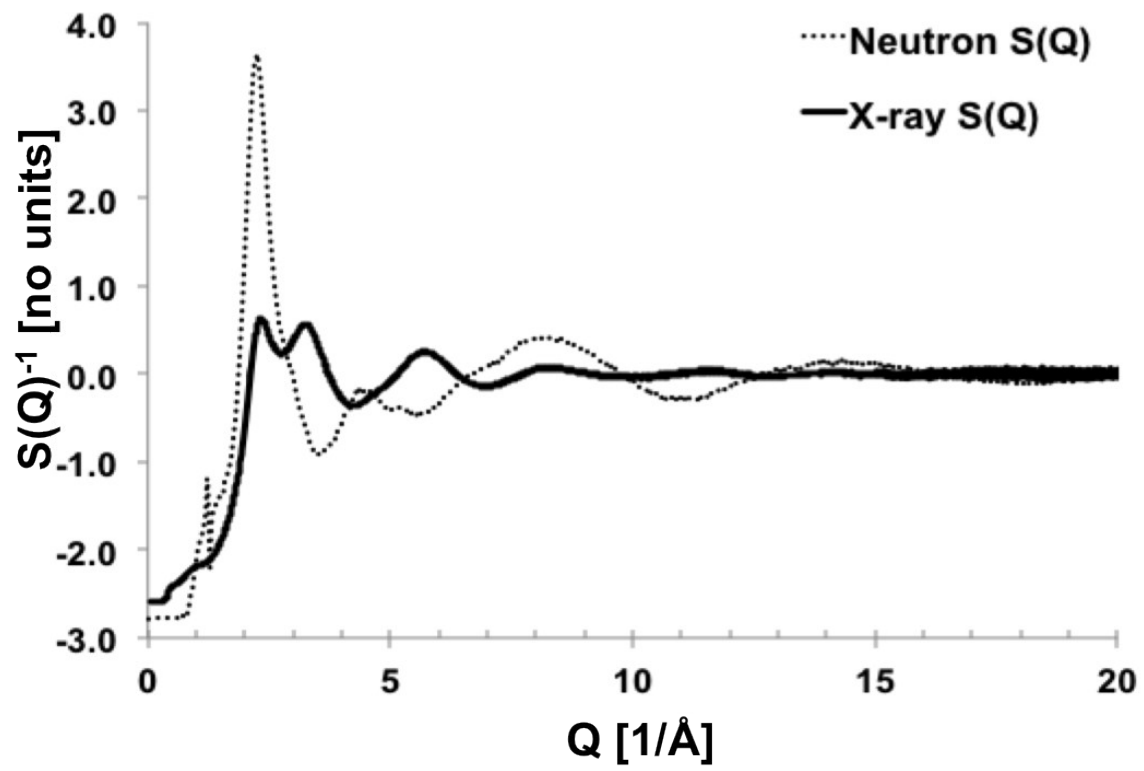


Figure S5. Pie chart of percent observation of different local configuration solvation environments about OH^- and Na^+ predicted in the non-polarizable simulation

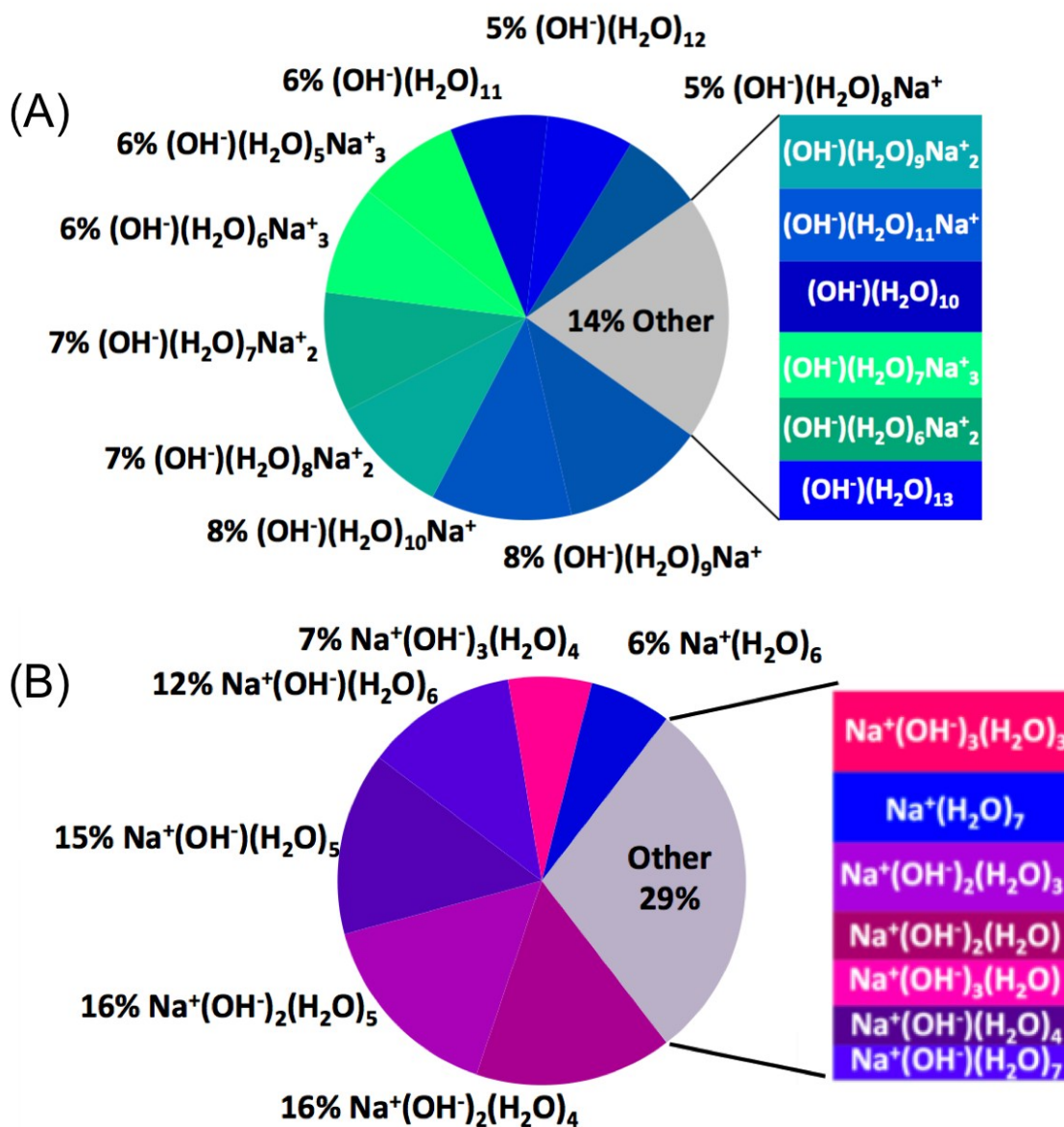


Table S4. Atom-atom contributions to RDF's at 2.4 Ang

Pair	Ow-Dw		Ow-Dd		Ow-Na		Od-Dw		Od-Dd		Od-Na		Ow-Ow		Ow-Od	
	opls	Pol.														
RDF peak @ 2.4 Å	0.28	0.21	0	0.25	0.05	4.13	1.23	0.11	0.18	0.39	7.54	5.26	0	0		0
int(RDF)	0.69	1.03	0	0.1	0.68	0.37	0.55	0.74	0.03	0.04	0.32	1.36	0	0		0

Table S5. Atom-atom contributions to RDF's at 2.66 Ang

Pair	Ow-Dw		Ow-Dd		Ow-Na		Od-Dw		Od-Dd		Od-Na		Ow-Ow		Ow-Od	
	opls	Pol.														
RDF peak @ 2.66 Å	1.11	0.74	6.70	0.25	0.07	1.58	1.39	0.20	0.25	0.41	1.82	0.13	0.96	1.43	6.5	4.96
int(RDF)	1.57	1.49	0.49	0.14	0.69	0.75	5.5	3.3	0.07	0.10	1.33	1.53	0.19	0.19	0.5	0.25

Table S6. Hydrogen bond distributions (% observation) for H₂O and OH⁻ from polarizable and non-polarizable simulations at $\chi = 0.245$ NaOH_(aq), where * indicates the molecule of reference.

# of HBs	H ₂ O*...H ₂ O		H ₂ O*...HO ⁻		HO ⁻ *...H ₂ O	
	Pol.	Non-pol.	Pol.	Non-pol.	Pol.	Non-pol.
0	31	36	78	40	2	2
1	37	42	19	43	15	13
2	26	19	3	15	36	24
3	5	3	0.3	2	37	29
4					9	17
5					0.4	10
6						1
7						

References:

- 1 J. Neufeind, M. Feygenson, J. Carruth, R. Hoffmann and K. K. Chipley, *Nucl. Instruments Methods Phys. Res. Sect. B Beam Interact. with Mater. Atoms*, 2012, **287**, 68–75.
- 2 A. P. Hammersley, S. O. Svensson, M. Hanfland, A. N. Fitch and D. Hausermann, *High Press. Res.*, 1996, **14**, 235–248.
- 3 X. Qiu and S. J. L. Billinge, *J. Appl. Crystallogr.*, 2004, **37**, 678.
- 4 P. J. Chupas, X. Qiu, J. C. Hanson, P. L. Lee, C. P. Grey and S. J. L. Billinge, *J. Appl. Crystallogr.*, 2003, **36**, 1342–1347.
- 5 E. Lorch, *J. Phys. C Solid State Phys.*, 1969, **2**, 229–237.
- 6 A. K. Soper and E. R. Barney, *J. Appl. Crystallogr.*, 2011, **44**, 714–726.
- 7 A. K. Soper, *Mol. Phys.*, 2009, **107**, 1667–1684.
- 8 J. P. Ryckaert, G. Ciccotti and H. J. C. Berendsen, *J. Comput. Phys.*, 1977, **23**, 327–341.
- 9 S. Nosé, *J. Chem. Phys.*, 1984, **81**, 511–519.
- 10 W. G. HOOVER, *Phys. Rev. A*, 1985, **31**, 1695–1697.
- 11 W. C. Swope, H. C. Andersen, P. H. Berens and K. R. Wilson, *J. Chem. Phys.*, 1982, **76**, 637–649.
- 12 J. Mesot, *Neutron News*, 1992, **3**, 29.
- 13 P. A. Doyle and P. S. Turner, *Acta Crystallogr. Sect. A*, 1968, **24**, 390–397.
- 14 E. N. Maslen, A. G. Fox and M. A. O’Keefe, in *International Tables for Crystallography Volume C: Mathematical, physical and chemical tables*, ed. E. Prince, Dordrecht ; Boston ; London :Published for the International Union of Crystallography by Kluwer Academic Publishers, 2004.
- 15 A. Ozkanlar and A. E. Clark, *J. Comput. Chem.*, 2014, **35**, 495–505.
- 16 G. Pálinkás, T. Radnai and F. Hajdu, *Zeitschrift fur Naturforsch. - Sect. A J. Phys. Sci.*, 1980, **35**, 107–114.
- 17 H. Ohtaki and T. Radnai, *Chem. Rev.*, 1993, **93**, 1157–1204.
- 18 R. Caminiti, G. Licheri, G. Paschina, G. Piccaluga and G. Pinna, *J. Chem. Phys.*, 1980, **72**, 4522–4528.
- 19 J. Mähler and I. Persson, *Inorg. Chem.*, 2012, **51**, 425–438.
- 20 R. Mancinelli, A. Botti, F. Bruni, M. A. Ricci and A. K. Soper, *J. Phys. Chem. B*, 2007, **111**, 13570–13577.
- 21 T. Megyes, S. Bálint, T. Grósz, T. Radnai, I. Bakó and P. Sipos, *J. Chem. Phys.*, 2008, **128**, 44501.
- 22 M. Galib, M. D. Baer, L. B. Skinner, C. J. Mundy, T. Huthwelker, G. K. Schenter, C. J. Benmore, N. Govind and J. L. Fulton, *J. Chem. Phys.*, 2017, **146**, 84504.
- 23 M. E. Tuckerman, D. Marx and M. Parrinello, *Nature*, 2002, **417**, 925.
- 24 A. Botti, F. Bruni, S. Imberti, M. A. Ricci and A. K. Soper, *J. Chem. Phys.*, 2004, **120**, 10154–10162.
- 25 D. Marx, A. Chandra and M. E. Tuckerman, *Chem. Rev.*, 2010, **110**, 2174–2216.
- 26 I. S. Ufimtsev, A. G. Kalinichev, T. J. Martinez and R. J. Kirkpatrick, *Chem. Phys. Lett.*, 2007, **442**, 128–133.
- 27 J. S. Hub, M. G. Wolf, C. Caleman, P. J. Van Maaren, G. Groenhof and D. Van Der Spoel, *Chem. Sci.*, 2014, **5**, 1745–1749.
- 28 C. D. Wick and L. X. Dang, *J. Phys. Chem. A*, 2009, **113**, 6356–6364.
- 29 H. J. C. Berendsen, J. R. Grigera and T. P. Straatsma, *J. Phys. Chem.*, 1987, **91**, 6269–6271.

- 30 W. L. Jorgensen, 'OPLS all-atom parameters for organic molecules, ions, & nucleic acids, July 2008' as provided by W. L. Jorgensen, Yale University during June 2009 and consulted on J. W. Ponder <https://dasher.wustl.edu/tinker/distribution/params/opsaa.prm> on 18 December, <http://zarbi.chem.yale.edu/opsaam.html>.
- 31 G. Lamoureux, E. Harder, I. V. Vorobyov, B. Roux and A. D. MacKerell, *Chem. Phys. Lett.*, 2006, **418**, 245–249.
- 32 Y. Luo, W. Jiang, H. Yu, A. D. MacKerell and B. Roux, *Faraday Discuss.*, 2013, **160**, 135–149.

